Triplet-Triplet Upconversion in Organic Light-Emitting Diodes: Implications to Injection Lasing

Atul Shukla
University of Queensland https://orcid.org/0000-0001-7453-5815
Monirul Hasan
University of Queensland
Gangadhar Banappanavar
Department of Physics, Indian Institute of Technology Bombay,
Viqar Ahmad
University of Queensland https://orcid.org/0000-0002-6782-7382
Jan Sobus
University of Queensland
Evan Moore
University of Queensland
Dinesh Kabra (dkabra@gmail.com)
Department of Physics, Indian Institute of Technology Bombay,
Shih-Chun Lo (s.lo@uq.edu.au)
University of Queensland https://orcid.org/0000-0002-4634-5376
Ebinazar Namdas (e.namdas@uq.edu.au)
University of Queensland https://orcid.org/0000-0001-5761-495X

Article

Keywords: amplified spontaneous emission, triplet-triplet upconversion, anthracene derivatives, organic light-emitting diode, deep-blue emission

Posted Date: September 15th, 2020

DOI: https://doi.org/10.21203/rs.3.rs-74957/v1

Triplet-Triplet Upconversion in Organic Light- Emitting Diodes: Implications to Injection Lasing

Atul Shukla,[a,b] Monirul Hasan, [a,b] Gangadhar Banappanavar,[d] Viqar Ahmad,[a,b] Jan Sobus,[a,b] Evan G. Moore,[c] Dinesh Kabra,[d,*] Shih-Chun Lo,[a,c,*] Ebinazar B. Namdas [a,b,*]

[a] Centre for Organic Photonics & Electronics, The University of Queensland, Brisbane, Queensland 4072, Australia

[b] School of Mathematics and Physics, The University of Queensland, Brisbane, Queensland 4072, Australia.

[c] School of Chemistry and Molecular Biosciences, The University of Queensland, Brisbane, Queensland 4072, Australia.

[d] Department of Physics, Indian Institute of Technology Bombay, Mumbai 400076, India

[*]Correspondence to: Ebinazar B. Namdas (e.namdas@uq.edu.au)

Shih-Chun Lo (s.lo@uq.edu.au)

Dinesh Kabra (dkabra@iitb.ac.in)

Keywords: amplified spontaneous emission, triplet-triplet upconversion, anthracene derivatives, organic light-emitting diode, deep-blue emission

ABSTRACT

While significant progress has been made over last few years in the field of organic solid-state lasers, achieving lasing action from organic semiconductors under electrical excitation still remains a big challenge. One of the major barriers towards electrically pumped organic lasers are optical losses due to triplet excitons. In this work, we report both experimental and theoretical results that confirm positive contribution of triplet excitons for the scope of electrically driven organic laser. We studied a model fluorescence material, 9-(9-phenylcarbazole-3-yl)-10(naphthalene-1-yl) anthracene and reveals that the threshold current densities required to achieve lasing emission under electrical injection can be significantly reduced with the aid of triplet-triplet exciton upconversion processes. Furthermore, we demonstrate that, to achieve the best performance, the singlet-triplet exciton annihilation must be minimized. These results are unprecedented and provide a pathway towards development of new class of triplet-triplet upconversion materials for injection laser.

1. Introduction

Light-emitting optoelectronic devices based on organic semiconductors such as organic light-emitting diodes (OLEDs)[1-3] and light-emitting field-effect transistors (LEFETs)[4-6] have shown promising advancements in last two decades towards applications in areas such as high-end TVs, flexible display technology, low-cost solid-state lighting and data communications.[4,7] Organic solid state-state lasers (OSSLs) on the other hand have received significant attention in recent years because of their ability to provide tunable, coherent light emission while allowing compatibility with a variety of substrates such as silicon, ITO/glass or plastic at low cost processing techniques. At the moment, most of the OSSLs are optically pumped using a pulsed excitation source with pulse widths ranging from femtoseconds (fs) to few nanoseconds (ns).[8-14] Furthermore, lasing under electrical excitation can open up new prospects for next

generation display, biomedical sensor and lighting applications with unprecedented color purity. These lasers can seamlessly integrate with existing manufacturing ecosystem such as CMOS, OLEDs display and printing technologies. Recently, Sandanayaka *et al.* demonstrated indication of lasing emission under electrical pumping using 4,4′-bis[(*N*-carbazole)styryl]biphenyl (BSBCz) as the organic laser gain medium.[15] However, the devices demonstrated in the study were found to be unstable due to the high driving voltages required to achieve lasing emission. Hence, further studies towards development of new materials for electrically pumped organic lasers are much required.

Achieving lasing emission under electrical excitation is a difficult task. This is primarily because of the trade off in photoluminescence quantum yields (PLQYs) and charge carrier mobility of organic materials.[16] Obtaining high mobility in organic compounds essentially requires higher degree of π-π stacking between the chromophores in films, this in turn leads to drastic reduction in PLQYs due to aggregate induced luminescence quenching.[17] To overcome this, molecular doping approach has been employed to achieve high film PLQYs, low lasing threshold (E_{th}) and high efficiency in case of optically pumped laser and OLEDs.[18] However, doping approach leads to reduction in charge carrier mobility of these systems. Apart from high mobility and high PLQY, organic laser gain medium should also possess high radiative rate constant (k_r) and high electroluminescence (EL) quantum yield in order to achieve lasing action at low optical pump intensities and hence at low injection current densities. To address these issues, continuous efforts are made to obtain high EL efficiency from non-doped fluorescent emitters with high radiative rate constants.[19] Unfortunately, the maximum internal quantum efficiency (IQE) of OLEDs based on fluorescent materials is limited only to 25%. On the other hand, OLEDs based on phosphorescent and recently developed materials utilizing thermally activated delayed fluorescence (TADF)[20] provide 100% IQEs. However, these materials do not give stimulated emission due to long excited-

state lifetimes and low radiative rates. Hence, it is crucial to discover new classes of light-emitting materials that can possess high k_r and high EL quantum yield in order to achieve lasing action from organic semiconductors at low current densities. Anthracene derivatives have been one of the most extensively studied materials, which show efficient EL and charge transport properties in non-doped conditions in OLEDs.[21-27] Anthracene derivatives in OLEDs have continuously showed high external quantum efficiencies (EQEs) exceeding the theoretical limit of traditional fluorescent emitters for past several years.[22-24,28-30] This is mostly attributed to the triplet-triplet upconversion (TTU) in these anthracene derivatives. Furthermore, recently Adachi *et al.* reported enhancement in TTU efficiency of anthracene derivatives close to 50% through spin-orbit coupling leading to high IQEs of close to 60%.[31] The TTU enhanced efficiency of the anthracene derivatives is promising for application in injection lasing. However, the influence of TTU in OSSLs has not yet been explored.

In this work, we investigate the EL and light amplification properties of one such model anthracene derivative 9-(9-phenylcarbazole-3-yl)-10(naphthalene-1-yl) anthracene (PCAN) with chemical structure shown in **Figure 1a**.[32-35] The performance of PCAN based OLEDs in neat and doped conditions were studied under steady state and nanosecond pulsed excitation. We found that high EQEs of this material in non-doped conditions can be attributed to TTU at low current densities (J) while at higher current densities singlet-triplet annihilation (STA) becomes a detrimental factor leading to sharp EQE roll-off. We performed time-resolved photoluminescence spectroscopy (TRPL), fluence dependence study for prompt (PF) and delayed fluorescence (DF) and nanosecond-transient absorption spectroscopy (ns-TAS) to extract rate constants and to understand the various bimolecular recombination processes. Furthermore, we performed theoretical modelling to extract rate STA and TTU rate constants. To gain information on lasing, amplified spontaneous emission (ASE) characteristics were measured for doped and neat films of PCAN under nanosecond-optical excitation. Using the

exciton-exciton annihilation parameters, the current density required to achieve the lasing threshold were then simulated. We show that the high TTU rate constant can lead to significant reduction in threshold current density required to achieve lasing emission under electrical excitation. This study also highlights, STA rate constants need to be reduced significantly alongside increment in TTU rate constants in future material design. To the best of our knowledge, this is the first comprehensive study on TTU material that sheds light into interplay between triplet up-conversion, singlet-triplet annihilation and lasing threshold.

2. Results and Discussion

2.1. Steady-state photophysical properties

Photophysical properties of PCAN were studied in toluene solution, neat and doped films (10wt% PCAN in 4,4′-bis(*N*-carbazolyl)-1,1′-biphenyl (CBP)). As shown in previous theoretical study, the highest occupied molecular orbital (HOMO) and lowest occupied molecular orbital (LUMO) are primarily delocalized on the anthracene unit along non-planar (tilted by close to 90º) orientation of the 9, 10 substituents, which allows to maintain the electronic structure of anthracene while the non-planar structure helps in reducing the aggregate induced photoluminescence quenching as compared to other anthracene derivatives.[32] **Figure 1b** shows the normalised absorption and photoluminescence spectra of PCAN in dilute toluene solution, neat films and doped films. The absorption spectra of PCAN in solution and neat films show typical vibronic structures arising from the anthracene unit while absorption spectra in the doped films is majorly dominated by the absorption of CBP host. The PL spectrum of PCAN in solution shows major emission wavelength peak at 428 nm along with a slight shoulder at 445 nm. On the other hand, PL spectrum for the neat film was found to be red-shifted with emission peak at 452 nm, compared to that of solution. The red shift in emission of neat film can be attributed to the intermolecular interaction in neat films,

which is absent in dilute solutions.[16] The emission spectra in doped films also showed major peak at 452 nm, though the contribution of shoulder at 435 nm was found to be enhanced in doped film, suggesting that the intermolecular interaction in doped films are significantly reduced as compared to the neat films. The above features of the PL spectra are further supported by the PLQY values. The PLQY of dilute toluene solution was found to be 64±7%, while for neat films this value drops down to 37±6%. However, doping in CBP host helps in retaining the high PLQY value of 54±6% for this system.

2.2. OLED characteristics

To understand the EL properties, we fabricated OLEDs with non-doped and 10wt% PCAN doped in CBP host as the emissive layer (EML). The structure of fabricated OLEDs consisted of indium tin oxide (ITO)/PEDOT:PSS (40 nm)/NPB (20 nm)/EML (40 nm)/Alq_3 (20 nm) /LiF (0.8 nm)/Al (100 nm), where PEDOT:PSS = poly(3,4-ethylenedioxythiophene): poly(styrenesulfonate), NPB = *N*,*N*'-bis(naphthalene-1-yl)-*N*,*N*'-bis(phenyl)-benzidine, Alq_3 = tris(8-hydroxy-quinolinato) aluminium. In order to obtain better electron injection in doped film devices 1,3,5-tris(1-phenyl-1*H*-benzimidazol-2-yl) benzene (TPBi) was used as the electron transport layer instead of Alq_3.

Figure 2a shows the EQE as a function of current densities for neat and doped films. OLEDs based on doped films showed sharp EQE roll-off with increasing current density while non-doped devices show a "roll-up" in EQE with increasing current densities till 20 mA cm^{-2}. The current density and luminance *versus* voltage (*J-V-L*) characteristics and EL spectra of PCAN based doped and non-doped OLEDs, respectively, are shown in **Figure S1a-c** (in the Supporting Information). **Table S1** shows the performance comparison of PCAN based doped and non-doped devices. Even though the peek EQE of 2.8% at 1600 cd/m^2 achieved in this study for non-doped devices was found to be slightly lower than the reported EQE for PCAN,[32]

it is interesting to note that peak EQE still exceeds the theoretical EQE limit of ≈1.9% for typical fluorescent OLEDs (calculated from the neat-film PLQY of 37%, assuming singlet: triplet generation of 1:3 and light out-coupling of 20%). Devices with doped PCAN EMLs on the other hand showed a peak EQE of ≈2.3% at 1 cd/m^2, which is lower than that achieved with non-doped devices and also lower than the theoretical fluorescent limit (≈2.75%) even despite the doped EML by having a higher PLQY (≈55%). These results suggest a vital contribution of triplet to singlet up-conversion in non-doped devices, which is otherwise absent or significantly reduced in doped devices, leading to superior performance of non-doped PCAN OLEDs. Furthermore, the absence of any strong donor-acceptor moieties in the molecular structure dismisses the presence of TADF or "hot exciton" channel, which can be mediated *via* hybrid charge transfer-locally excited (HLCT) character of singlet and higher lying triplet states.[36-38]

Figure 2b shows the comparison of luminance *versus* current density plots (log-log scale) for doped and non-doped devices. Herein, doped devices show characteristics typical to fluorescent OLEDs with slope close to 1. This suggested a linear relationship between output photons and excitons generated. Non-doped devices on the other hand show two regimes with a slope of ≈1.3 under low current densities and a slope of ≈1 when current densities are increased. As seen in previous studies,[39] this non-linear relationship (slope >1 in log-log plots) between luminance and current density is the typical characteristics of up-conversion of triplet excitons to singlet excited-states *via* TTU process.

2.3. TRPL and fluence dependent measurements

To obtain insight into the non-linear relationship (slope >1) between luminance and current density in PCAN neat-film devices, we studied the time resolved characteristics of PCAN under optical excitation. **Figure S2** shows the time correlated single photon counting (TCSPC) decay curves at peak PL wavelengths for PCAN in dilute toluene solution, neat and

10wt% doped in CBP films. In dilute toluene solution (deoxygenated), the fluorescence intensity decays mono-exponentially with lifetime of 3.5 ns. However, the neat and doped films showed bi-exponential decay in prompt fluorescence (PF) along with small contributions from delayed fluorescence (DF) in the longer times. The details of the lifetime and their respective contributions are listed in **Table S2**. For neat films, the fast components of 1.1 ns (81%) and 3.5 ns (14%) in the PF can be attributed to aggregates and non- aggregate state respectively. While the presence of long lived (~ 85 ns) DF is a characteristic feature observed in case of up-conversion of triplet excitons to singlet excited-states *via* TTU process[40].

To further study the long-lived DF in neat and doped films, we used variable gate-delays (ranging from picosecond to microsecond range) based TRPL technique. **Figure 3a** shows the complete PL decay kinetics of neat and doped films excited at 355 nm (840 ps pulse width) laser source with excitation fluence of 80 μJ cm^{-2}. The neat films show distinct long-lived DF, compared to the doped films. Interestingly, neat films showed two DF regions with lifetime in order of several hundreds of ns (black solid line) and 10 μs (blue solid line), respectively. We attribute the origin of the two DFs in neat films to different triplet diffusivity due to different orientations of chromophores in the bulk. Similar impact of molecular packing on DF has been previously observed for several systems.[41] **Figure 3b** shows the PL spectra for neat films at different gate delays. The similarity in spectra for PF and DF confirms that both emissions arise from the same excited-state species.

To confirm the TTU under optical excitation, we have carried out time resolved fluence dependence PL and carefully monitor the relative contribution of DF and PF. **Fig. 3c** shows normalised DF intensities as a function of normalised PF intensities at same pump fluence. Herein, the absolute PF and DF intensities were obtained by integrating the respective spectra over all wavelengths. We note that under lower fluence region, both PF and DF follow almost linear relationship and then start to shift towards almost quadratic relation at higher pump

fluence. This is due to fact that increment of triplet excited-state population with increasing fluence leads enhancement in contribution due to TTU. The near quadratic relation in fluence dependent studies confirm the presence of TTU, which is consistent with non-linear relation of luminance and current density under electrical excitation.

2.4. Nano second Transient electroluminescence studies

To obtain a complete picture of TTU which contribute to EQE "roll-up" processes, we studied the transient electroluminescence at high current densities. The OLEDs were subjected to 100 ns electrical pulse at high current density. The prime benefits of applying a short pulse to the OLED is suppression of the joule heating. The schematic of the transient EL setup is shown in **Figure S3**. The device areas of the OLEDs were reduced to 0.3 mm^2 to minimise the RC response distortion by reducing the geometrical capacitance. **Figure S4a** and **b** shows the transient current density and EL intensity in non-doped and doped PCAN based OLEDs, respectively (under 100 ns voltage pulse). Contrary to DC results in **Section 2.2**, where the operation of OLEDs is limited to low current densities (<1 A cm^{-2}), higher current densities (>2.6 A cm^{-2}) were used under pulsed excitation. Current response of both doped and non-doped OLED show sharp rise (typical response under space charge limited current (SCLC) conditions) and reaches steady state after 15 ns (**Figure S4**). **Figure 4a** and **b** depicts the normalised EL transients for non-doped and doped devices, respectively, at 20 and 40 V. For non-doped devices at 20 V, EL intensity shows a sharp rise after 25 ns, followed by gradual increment as the time progresses while at 40 V, EL intensity peaks and then rapidly reduces down 73% of the initial intensity. The EL intensity here is representative of the singlet excitons, the gradual rise with time in EL intensity at 20 V indicates the triplet to singlet up-conversion due to TTU, while the rapid reduction of intensity at 40 V is a signature of dominating STA, leading to reduction in singlet density. STA dominates primarily *via* Förster-type energy

transfer mechanism, whose efficacy is determined by the spectral overlap between S_1 emission and $T_1 \rightarrow T_n$ absorption bands.

To confirm STA in PCAN, we performed nano-second transient optical pump-probe absorption spectroscopy. **Figure S5** shows the triplet and singlet excited-state absorptions for neat PCAN films measured under vacuum. The long-lived triplet excited-state absorption band positioned between 400–500 nm was found to overlap strongly with the emission confirming STA in PCAN. **Figure S6** further shows the normalised EL turn-off characteristics for doped and non-doped devices at 20 V, showing prompt and delayed components.

Next, we quantitatively extracted the STA and TTU rate constants from singlet and triplet population using rate equations designed for anthracene derivatives (details in the Supporting Information **Section S1**). **Figure 5a** and **b** shows the theoretical fits and the corresponding triplet population density for non-doped and doped devices, respectively at 20 and 40 V. From EL transients, STA and TTU rate constants for doped devices are obtained as 1.44×10^{-9} cm^3 s^{-1}, and $6.67 \times 1\ 0^{-11}$ cm^3 s^{-1}, respectively (**Table S4**). The extracted annihilation rate constants for non-doped PCAN devices are significantly higher than the doped PCAN devices with a value of 7.37×10^{-9} cm^3 s^{-1} for STA and 2.32×10^{-10} cm^3 s^{-1} for TTU (**Table S3**). These rate constant are well within the typical range of STA and TTU rate constants reported for organic semiconductors in the literature.[42] Clearly, the STA rate constant for the non-doped devices is much higher than typical fluorescent OLED emitters but this is still lower than those reported for anthracene single crystals.[43] The higher value of TTU rate constant in non-doped devices explains the higher peak EQEs, compared to doped devices at steady-state condition as contribution from delayed fluorescence is significantly enhanced. However, the higher STA rate constant in non-doped devices implies a trade-off between TTU and STA.[41,44-47]

2.5. Light amplification properties

To study the light amplification properties of PCAN, we explored the ASE characteristics for PCAN neat and doped films. ASE characteristics were obtained by optically exciting the samples using nitrogen laser with pulse width of 3.5 ns at 337 nm. The emission from the edge of the samples was collected using a spectrometer. The ASE threshold (E_{th}) was obtained from the abrupt change of slope in plots of output intensity from the edge of the sample *vs* input excitation fluence along with drop in full width at half maxima (FWHM) of the output spectra. **Figure 6a** and **b** shows the typical input-output-FWHM plots and emission spectra at various intensities for neat and doped films, respectively. The ASE lasing threshold for doped and neat films were 16 μJ cm^{-2} and 500 μJ cm^{-2} respectively. The light amplification in TTU based emitter is very encouraging. However, the key question is, whether TTU based material is beneficial under electrical injection, a critical figure-of-merit for development of electrically pumped organic lasers.

The ASE threshold measured above can be translated into threshold singlet exciton density by employing optical model similar to the one described in **Section S1** (details in the Supporting Information **Section S2**). The threshold singlet exciton density was found to be 3 × 10^{19} cm^{-3} and 1 × 10^{18} cm^{-3} for neat and doped films, respectively. We then extract the threshold current density (J_{th}) required to reach this singlet exciton density under electrical excitation (details in the Supporting Information **Section S2**). For comparative analysis, we considered three conditions: 1) an ideal case with no annihilation of singlet-singlet (SSA), singlet-triplet (STA) and triplet-triplet (TTU) excitons; 2) when only STA and 3) when both STA and TTU are taken in account. Using the k_{STA} and k_{TTU} values extracted in **Section 2.4**, we calculated the singlet exciton density as the function of current density in all the three conditions. **Figure 7a** and **b** shows the calculated singlet exciton density as the function of current density for doped and neat systems, respectively, with threshold singlet exciton density

for lasing shown by horizontal blue line. It is interesting to note that when only STA is considered, the singlet population do not reach the threshold required to achieve lasing in both doped as well as non-doped system. This suggest that the losses due STA are extremely detrimental to lasing. When both STA and TTU rate constants are considered, the singlet population can reach the threshold of current density, $J_{th} \sim 40$ kA cm^{-2} for doped devices. These results highlight the positive impact of TTU on reducing the J_{th} required to achieve lasing in organic semiconductors.

To further elucidate the impact of STA and TTU on lasing threshold, we varied k_{TTU} in range 10^{-11} -10^{-10} and k_{STA} in range 10^{-9}-10^{-8} and simulated the J_{th} in doped PCAN devices while keeping the other rate constants unchanged. **Figure 8**, shows the simulated values of J_{th} as a function of k_{TTU} and k_{STA} values. As k_{TTU} is increased, J_{th} reduces gradually. In contrast, J_{th} increases rapidly as k_{STA} increases. Comparison of J_{th} values as a function of linear increase in k_{TTA} and k_{STA} is further depicted in **Figure S7**. Clearly, the STA has much severe detrimental impact on J_{th}, whereas TTU facilitates in reducing the lasing threshold. Thus, TTU plays a crucial role in reducing the injection lasing threshold. However, STA must also be simultaneously minimized to obtain the best performance. The way to reduce the STA is by designing TTU material that has minimum spectral overlap between singlet emission and triplet absorption spectrum. Other probable techniques include, the use of dual core TTU chromophores[48] with high up-conversion yield and utilizing materials with high TTU efficiency as a host matrix that can lead to enhancement in EL properties of existing high-performance organic laser dyes.[49-52]

3. Conclusion

In summary, we report both experimental and theoretical results that confirm positive contribution of TTU for the scope of electrically driven organic laser. We selected, PCAN as a model material exhibiting efficient triplet-triplet up-conversion and showed light

amplification properties under optical pulse excitations. We studied the transient EL response of PCAN OLEDs and demonstrated that triplet population plays a critical role in controlling the device efficiency as a function of current density through TTU and STA processes. Furthermore, by theoretical modelling we showed that the threshold current densities required to achieve light amplification can be significantly reduced with the aid of TTU. We believe that these results are of significant importance for developing a new class of TTU based laser material for injection lasing.

4. Experimental Section

Photophysical measurements: UV-visible absorption spectra for thin films and solutions were measured using Cary-5000 UV-Vis spectrometer. Horiba Jobin Yvon Fluoromax was used to measure PL spectra. Solution PLQYs were determined using Quinine sulphate in 0.1 M H_2SO_4 as the standard (PLQY = 55%) as the standard. Optical density of standard and the sample were measured to be 0.1 at excitation wavelength of 360 nm.[53] Solid-state PLQY measurements were performed using a calibrated integrating sphere.[54] Nano-second transient absorption spectroscopy (TAS) were performed as described in literature.[10] Pump wavelength of 400 nm was used to excite the sample. TCSPC measurements were performed using Halcyone fluorescence spectrometer with IRF (instrument response function) of 150 picoseconds (ps) with excitation wavelength 337 nm.

Thin film preparation: Thin films for photophysical and ASE measurements were prepared using same procedure. PCAN was purchased from LUMTEC and used as purchased. Non-doped and CBP doped films were deposited by thermal evaporation under high vacuum (~10^{-6} mbar) on pre-cleaned fused silica substrates to obtained thin films with 200 nm thickness as measure by Dektak 150 profilometer (Bruker). All the substrates were cleaned using acetone, isopropanol followed by UV-ozone.

Electrical Characterization: OLED for DC and pulse measurements were fabricated on top of pre-patterned and cleaned ITO-glass substrates with ITO thickness of 100 nm. Substrates were cleaned by ultrasonication in de-ionized water with Alconox for 15 minutes, followed by ultrasonication in de-ionized water, acetone and isopropanol for 5 minutes each. 40 nm of PEDOT: PSS (Ossila AI 4083) layer was spin-coated on top of ITO and annealed at 150 °C for 20 minutes. NPB (20 nm), EML (40 nm), TPBi/Alq_3 (20 nm), LiF (0.8 nm) and Al (100 nm) layers were sequentially deposited by thermal evaporation under high vacuum (~10^{-6} mbar). The DC *J-V-L* characteristics of the OLEDs (area~4 mm^2) were measured inside nitrogen filled glovebox using a Keithley 2400 source meter and absolute EQE measurement setup (Hamamatsu photonics C9920-12) with calibrated integrating sphere. Transient EL characteristics were measured by exciting the OLED devices (area ≈ 0.3 mm^2) using AVTECH pulse generator, AVX1011-B1-B, with rise and fall time of 2 ns. EL response was recorded with a calibrated photomultiplier tube (Hamamatsu, H10721–20), connected to a digital oscilloscope (Teledyne LeCroy, 2 GHz). Brightness was calculated using emission spectrum of the devices and taking in account calibration factor for the photomultiplier tube (assuming Lambertian emission).

TRPL measurements: For the time resolved spectroscopy the neat and doped films were mounted in the vacuum chamber with low pressure in the order of 10^{-5} mbar. Samples were excited at 355 nm using Nd: YAG INNOLAS LASER operating at 1 kHz repetition rate with 840 ps pulse width. Highly sensitive gated iStar Andor ICCD was used to collect the prompt and delayed emission.

ASE measurements: Randomly polarised nitrogen-gas laser (Stanford Instruments, NL-100) with emission wavelength of 337 nm and pulse width of 3.5 ns, operating at 20 Hz frequency was used to determine ASE characteristics. The laser was focused into a thin linear strip of dimension 0.5 × 0.01 cm^2 with the help of cylindrical lens and motorised slit. The samples

were kept under vacuum (~10^{-5} mbar) to prevent degradation during the measurements. Set of neutral density filters were used to tune the input excitation energy. Emission was collected from the edge of the samples using an optical fibre and spectrometer (Hamamatsu, Mini-spectrometer TM series, C10083CA) with spectral resolution of 5 nm.

Acknowledgments

The authors thank Department of Industry, Innovation and Science (AISRF53765) and Australian Research Council (DP200103036 and DP160100700) for funding this work. A.S. was supported by UQ's Research and Training Program, M.H. and V.A. were funded by Australian Postgraduate Award (APA). This work was performed in part at the Queensland node of the Australian National Fabrication Facility Queensland Node (ANFF-Q), a company established under the National Collaborative Research Infrastructure Strategy to provide nano- and microfabrication facilities for Australia's researchers. DK acknowledges DST-AISRF (No. DST/INT/AUS/P-74/2017) for funding support.

Author Contributions: A. S., S.-C.L. and E.B.N. conceived the idea of the manuscript. A.S., V.A., G.S.B, performed the experiments and analysed the results with the help of J.S. Theoretical model was developed by M.H. and A.S. under the guidance of E.B.N. M.H. fitted the experimental data with the full model and generated the simulated results. A.S. drafted the manuscript. E.G.M., D.K., S.-C.L. and E.B.N. supervised the work. All the authors contributed to data analysis and discussion of the results.

Data availability: The data that support the findings of this study are available from the authors upon request.

Code availability: The code used for simulations used in this study is available from the authors upon request

Competing Interests: The authors declare no conflict of interest

References

1 Tang, C. W. & VanSlyke, S. A. Organic electroluminescent diodes. *Applied Physics Letters* **51**, 913-915, doi:10.1063/1.98799 (1987).

2 Burroughes, J. H. *et al.* Light-emitting diodes based on conjugated polymers. *Nature* **347**, 539-541, doi:10.1038/347539a0 (1990).

3 Forrest, S. R. & Thompson, M. E. Introduction: Organic Electronics and Optoelectronics. *Chemical Reviews* **107**, 923-925, doi:10.1021/cr0501590 (2007).

4 Ahmad, V. *et al.* High-Speed OLEDs and Area-Emitting Light-Emitting Transistors from a Tetracyclic Lactim Semiconducting Polymer. *Advanced Optical Materials* **6**, doi:10.1002/adom.201800768 (2018).

5 Chaudhry, M. U. *et al.* Organic Light-Emitting Transistors: Advances and Perspectives. *Advanced Functional Materials*, doi:10.1002/adfm.201905282 (2019).

6 Hepp, A. *et al.* Light-emitting field-effect transistor based on a tetracene thin film. *Phys Rev Lett* **91**, 157406, doi:10.1103/PhysRevLett.91.157406 (2003).

7 Manousiadis, P. *et al.* in *2015 IEEE Summer Topicals Meeting Series (SUM)*. 222-223.

8 Mai, V. T. N. *et al.* Low Amplified Spontaneous Emission Threshold and Efficient Electroluminescence from a Carbazole Derivatized Excited-State Intramolecular Proton Transfer Dye. *ACS Photonics*, doi:10.1021/acsphotonics.8b00907 (2018).

9 Mamada, M., Fukunaga, T., Bencheikh, F., Sandanayaka, A. S. D. & Adachi, C. Low Amplified Spontaneous Emission Threshold from Organic Dyes Based on Bis-stilbene. *Advanced Functional Materials* **28**, doi:10.1002/adfm.201802130 (2018).

10 Shukla, A. *et al.* Deep-Red Lasing and Amplified Spontaneous Emission from Nature Inspired Bay-Annulated Indigo Derivatives. *Advanced Optical Materials* **8**, doi:10.1002/adom.201901350 (2019).

11 Karl, M. *et al.* Flexible and ultra-lightweight polymer membrane lasers. *Nat Commun* **9**, 1525, doi:10.1038/s41467-018-03874-w (2018).

12 Goossens, M., Ruseckas, A., Turnbull, G. A. & Samuel, I. D. W. Subpicosecond pulses from a gain-switched polymer distributed feedback laser. *Applied Physics Letters* **85**, 31-33, doi:10.1063/1.1767952 (2004).

13 McGehee, M. D. & Heeger, A. J. Semiconducting (Conjugated) Polymers as Materials for Solid-State Lasers. *Advanced Materials* **12**, 1655-1668, doi:doi:10.1002/1521-4095(200011)12:22<1655::AID-ADMA1655>3.0.CO;2-2 (2000).

14 Kuehne, A. J. & Gather, M. C. Organic Lasers: Recent Developments on Materials, Device Geometries, and Fabrication Techniques. *Chem Rev* **116**, 12823-12864, doi:10.1021/acs.chemrev.6b00172 (2016).

15 Sandanayaka, A. S. D. *et al.* Indication of current-injection lasing from an organic semiconductor. *Applied Physics Express* **12**, doi:10.7567/1882-0786/ab1b90 (2019).

16 Cornil, J., Beljonne, D., Calbert, J. P. & Brédas, J. L. Interchain Interactions in Organic π-Conjugated Materials: Impact on Electronic Structure, Optical Response, and Charge Transport. *Advanced Materials* **13**, 1053-1067, doi:10.1002/1521-4095(200107)13:14<1053::AID-ADMA1053>3.0.CO;2-7 (2001).

17 Liu, J. *et al.* High mobility emissive organic semiconductor. *Nat Commun* **6**, 10032, doi:10.1038/ncomms10032 (2015).

18 Kim, D.-H. *et al.* High-efficiency electroluminescence and amplified spontaneous emission from a thermally activated delayed fluorescent near-infrared emitter. *Nature Photonics* **12**, 98-104, doi:10.1038/s41566-017-0087-y (2018).
19 Baldo, M. A. & Forrest, S. R. Transient analysis of organic electrophosphorescence: I. Transient analysis of triplet energy transfer. *Physical Review B* **62**, 10958-10966, doi:10.1103/PhysRevB.62.10958 (2000).
20 Uoyama, H., Goushi, K., Shizu, K., Nomura, H. & Adachi, C. Highly efficient organic light-emitting diodes from delayed fluorescence. *Nature* **492**, 234-238, doi:10.1038/nature11687 (2012).
21 Xu, Y. *et al.* Highly Efficient Blue Fluorescent OLEDs Based on Upper Level Triplet-Singlet Intersystem Crossing. *Adv Mater* **31**, e1807388, doi:10.1002/adma.201807388 (2019).
22 Liu, W. *et al.* Nondoped blue fluorescent organic light-emitting diodes based on benzonitrile-anthracene derivative with 10.06% external quantum efficiency and low efficiency roll-off. *Journal of Materials Chemistry C* **7**, 1014-1021, doi:10.1039/c8tc05707a (2019).
23 Lim, H. *et al.* Enhanced Triplet-Triplet Annihilation of Blue Fluorescent Organic Light-Emitting Diodes by Generating Excitons in Trapped Charge-Free Regions. *ACS Appl Mater Interfaces* **11**, 48121-48127, doi:10.1021/acsami.9b15303 (2019).
24 Tang, X. *et al.* Efficient Nondoped Blue Fluorescent Organic Light-Emitting Diodes (OLEDs) with a High External Quantum Efficiency of 9.4% @ 1000 cd m−2 Based on Phenanthroimidazole−Anthracene Derivative. *Advanced Functional Materials* **28**, doi:10.1002/adfm.201705813 (2018).
25 Di, D. *et al.* Efficient Triplet Exciton Fusion in Molecularly Doped Polymer Light-Emitting Diodes. *Adv Mater* **29**, doi:10.1002/adma.201605987 (2017).
26 Yokoyama, D. *et al.* Dual efficiency enhancement by delayed fluorescence and dipole orientation in high-efficiency fluorescent organic light-emitting diodes. *Applied Physics Letters* **99**, doi:10.1063/1.3637608 (2011).
27 Chiang, C.-J. *et al.* Ultrahigh Efficiency Fluorescent Single and Bi-Layer Organic Light Emitting Diodes: The Key Role of Triplet Fusion. *Advanced Functional Materials* **23**, 739-746, doi:10.1002/adfm.201201750 (2013).
28 Peng, L. *et al.* Efficient soluble deep blue electroluminescent dianthracenylphenylene emitters with CIE y ($y \leq 0.08$) based on triplet-triplet annihilation. *Science Bulletin* **64**, 774-781, doi:10.1016/j.scib.2019.04.029 (2019).
29 Jayabharathi, J., Ramya, R., Thanikachalam, V. & Nethaji, P. Tailoring the molecular design of twisted dihydrobenzodioxin phenanthroimidazole derivatives for non-doped blue organic light-emitting devices. *RSC Advances* **8**, 29031-29043, doi:10.1039/c8ra05004j (2018).
30 Sung, M. J. *et al.* Dimethylsilyl-linked anthracene–pyrene dimers and their efficient triplet–triplet annihilation in organic light emitting diodes. *Journal of Materials Chemistry C* **5**, 1090-1094, doi:10.1039/c6tc05308d (2017).
31 Ieuji, R., Goushi, K. & Adachi, C. Triplet-triplet upconversion enhanced by spin-orbit coupling in organic light-emitting diodes. *Nat Commun* **10**, 5283, doi:10.1038/s41467-019-13044-1 (2019).
32 Cho, I., Kim, S. H., Kim, J. H., Park, S. & Park, S. Y. Highly efficient and stable deep-blue emitting anthracene-derived molecular glass for versatile types of non-doped OLED applications. *J. Mater. Chem.* **22**, 123-129, doi:10.1039/c1jm14482k (2012).
33 Ullah, M., Wawrzinek, R., Maasoumi, F., Lo, S.-C. & Namdas, E. B. Semitransparent and Low-Voltage Operating Organic Light-Emitting Field-Effect Transistors Processed

at Low Temperatures. *Advanced Optical Materials* **4**, 1022-1026, doi:10.1002/adom.201600050 (2016).

34 Ullah, M., Wawrzinek, R., Nagiri, R. C. R., Lo, S.-C. & Namdas, E. B. UV-Deep Blue-Visible Light-Emitting Organic Field Effect Transistors with High Charge Carrier Mobilities. *Advanced Optical Materials* **5**, doi:10.1002/adom.201600973 (2017).

35 Chaudhry, M. U. *et al.* Nano-Alignment in Semiconducting Polymer Films: A Path to Achieve High Current Density and Brightness in Organic Light Emitting Transistors. *ACS Photonics*, doi:10.1021/acsphotonics.8b00011 (2018).

36 Sharma, N. *et al.* Exciton efficiency beyond the spin statistical limit in organic light emitting diodes based on anthracene derivatives. *Journal of Materials Chemistry C* **8**, 3773-3783, doi:10.1039/c9tc06356k (2020).

37 Li, W. *et al.* A Twisting Donor-Acceptor Molecule with an Intercrossed Excited State for Highly Efficient, Deep-Blue Electroluminescence. *Advanced Functional Materials* **22**, 2797-2803, doi:10.1002/adfm.201200116 (2012).

38 Fu, C. *et al.* Highly efficient deep-blue OLEDs based on hybridized local and charge-transfer emitters bearing pyrene as the structural unit. *Chem Commun (Camb)* **55**, 6317-6320, doi:10.1039/c9cc02355k (2019).

39 Qiao, X., Yuan, P., Ma, D., Ahamad, T. & Alshehri, S. M. Electrical pumped energy up-conversion: A non-linear electroluminescence process mediated by triplet-triplet annihilation. *Organic Electronics* **46**, 1-6, doi:10.1016/j.orgel.2017.03.020 (2017).

40 Serevičius, T. *et al.* Triplet–Triplet Annihilation in 9,10-Diphenylanthracene Derivatives: The Role of Intersystem Crossing and Exciton Diffusion. *The Journal of Physical Chemistry C* **121**, 8515-8524, doi:10.1021/acs.jpcc.7b01336 (2017).

41 Dey, A. *et al.* Kinetics of thermally activated triplet fusion as a function of polymer chain packing in boosting the efficiency of organic light emitting diodes. *npj Flexible Electronics* **2**, doi:10.1038/s41528-018-0042-0 (2018).

42 Forget, S. & Chénais, S. in *Organic Solid-State Lasers* (eds Sébastien Forget & Sébastien Chénais) 13-73 (Springer Berlin Heidelberg, 2013).

43 Michel-Beyerle, M. E., Haberkorn, R., Kinder, J. & Seidlitz, H. Direct evidence for the singlet-triplet exciton annihilation in anthracene crystals. *physica status solidi (b)* **85**, 45-49, doi:10.1002/pssb.2220850103 (1978).

44 Zhang, Y. & Forrest, S. R. Triplets contribute to both an increase and loss in fluorescent yield in organic light emitting diodes. *Phys Rev Lett* **108**, 267404, doi:10.1103/PhysRevLett.108.267404 (2012).

45 Dey, A., Rao, A. & Kabra, D. A Complete Quantitative Analysis of Spatio-Temporal Dynamics of Excitons in Functional Organic Light-Emitting Diodes. *Advanced Optical Materials* **5**, doi:10.1002/adom.201600678 (2017).

46 Wallikewitz, B. H., Kabra, D., Gélinas, S. & Friend, R. H. Triplet dynamics in fluorescent polymer light-emitting diodes. *Physical Review B* **85**, doi:10.1103/PhysRevB.85.045209 (2012).

47 Dey, A. & Kabra, D. Role of Bimolecular Exciton Kinetics in Controlling the Efficiency of Organic Light-Emitting Diodes. *ACS Appl Mater Interfaces* **10**, 38287-38293, doi:10.1021/acsami.8b10559 (2018).

48 Hu, J.-Y. *et al.* Bisanthracene-Based Donor-Acceptor-type Light-Emitting Dopants: Highly Efficient Deep-Blue Emission in Organic Light-Emitting Devices. *Advanced Functional Materials* **24**, 2064-2071, doi:10.1002/adfm.201302907 (2014).

49 Pu, Y. J. *et al.* Optimizing the charge balance of fluorescent organic light-emitting devices to achieve high external quantum efficiency beyond the conventional upper limit. *Adv Mater* **24**, 1765-1770, doi:10.1002/adma.201104403 (2012).

50 Zhang, Y. & Forrest, S. R. Existence of continuous-wave threshold for organic semiconductor lasers. *Physical Review B* **84**, doi:10.1103/PhysRevB.84.241301 (2011).
51 Matsushima, T. *et al.* Degradation Mechanism and Stability Improvement Strategy for an Organic Laser Gain Material 4,4′-Bis[(N-carbazole)styryl]biphenyl (BSBCz). *Advanced Functional Materials* **29**, doi:10.1002/adfm.201807148 (2019).
52 Luo, Y. & Aziz, H. Correlation Between Triplet-Triplet Annihilation and Electroluminescence Efficiency in Doped Fluorescent Organic Light-Emitting Devices. *Advanced Functional Materials* **20**, 1285-1293, doi:10.1002/adfm.200902329 (2010).
53 Crosby, G. A. & Demas, J. N. Measurement of photoluminescence quantum yields. Review. *The Journal of Physical Chemistry* **75**, 991-1024, doi:10.1021/j100678a001 (1971).
54 Greenham, N. C. *et al.* Measurement of absolute photoluminescence quantum efficiencies in conjugated polymers. *Chemical Physics Letters* **241**, 89-96, doi:https://doi.org/10.1016/0009-2614(95)00584-Q (1995).

a)

b)

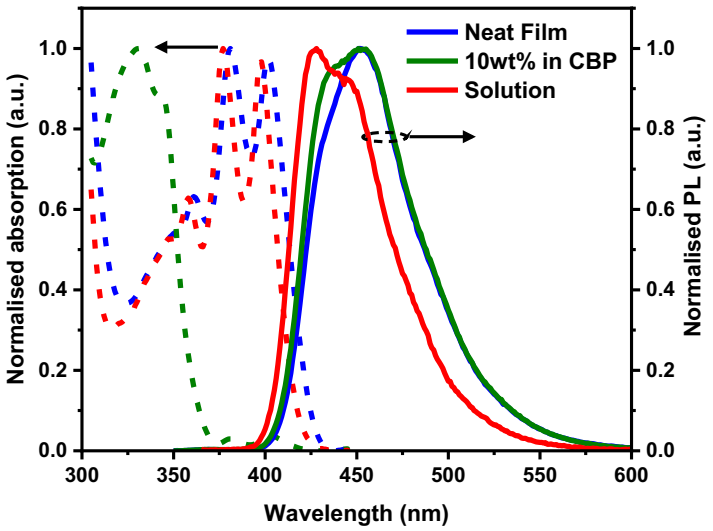

Figure 1. a) Chemical structure of PCAN. **b**) Normalised absorption (dashed lines) and PL (solid lines) spectra of PCAN in toluene solution (red), neat film (green) and 10wt% doped in CBP host matrix (blue).

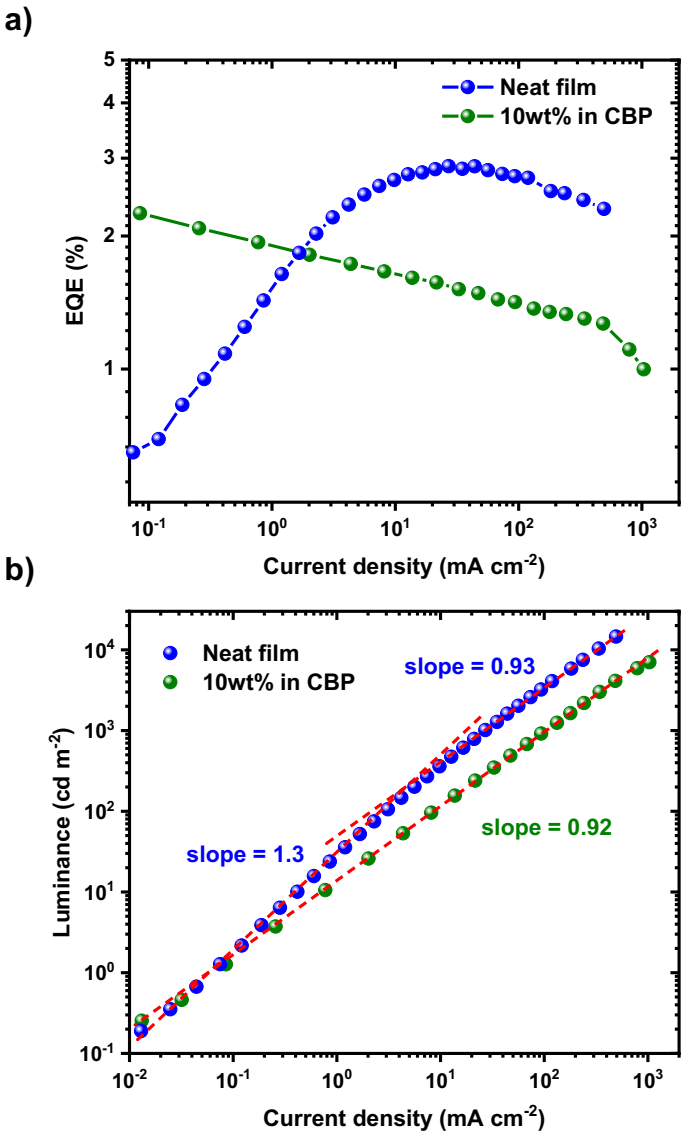

Figure 2. a) EQE *vs* current density and **b**) Luminance *vs* current density characteristics for OLEDs based on doped (green) and non-doped (blue) PCAN EMLs.

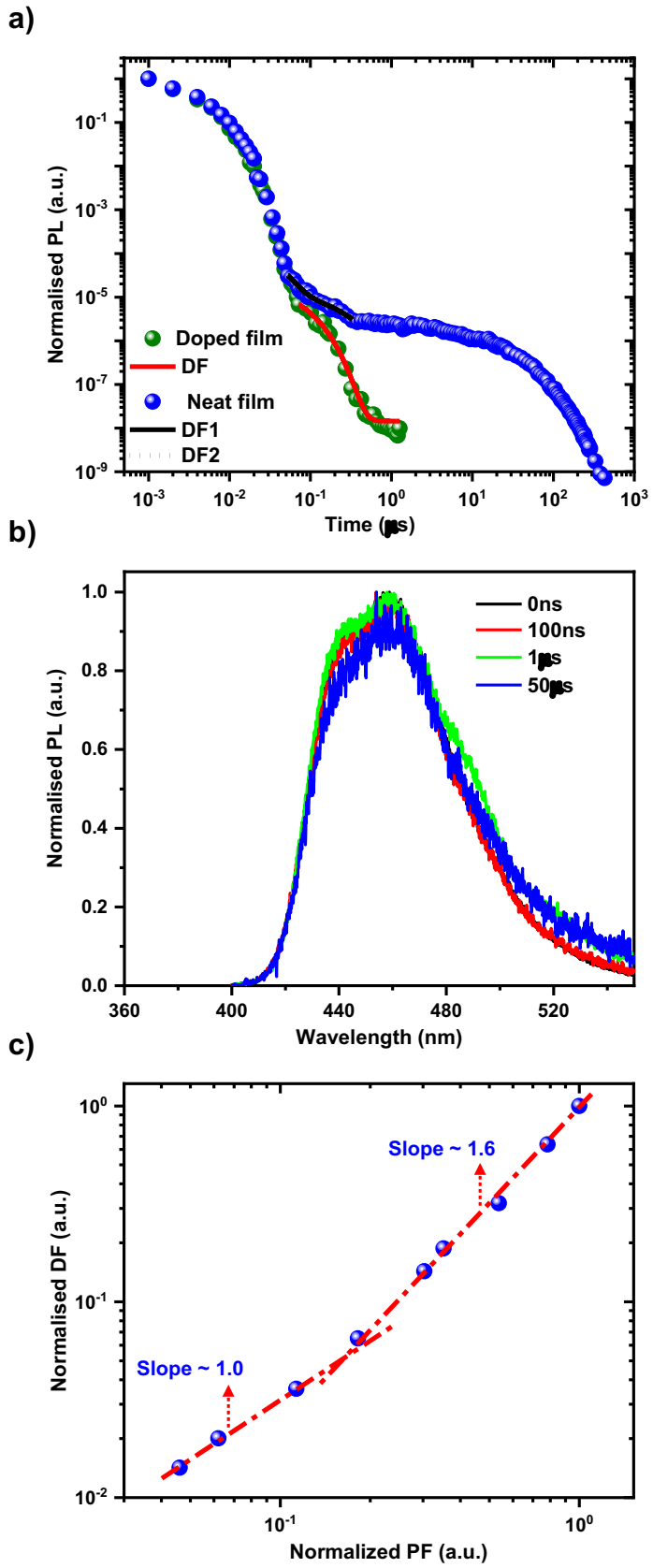

Figure 3. a) Time resolved emission decay for neat and doped films, **b**) emission spectra of neat films at different gate delays, **c**) Normalised DF intensities vs normalised PF intensities at different fluence for neat films, linearly fitted with dual slopes

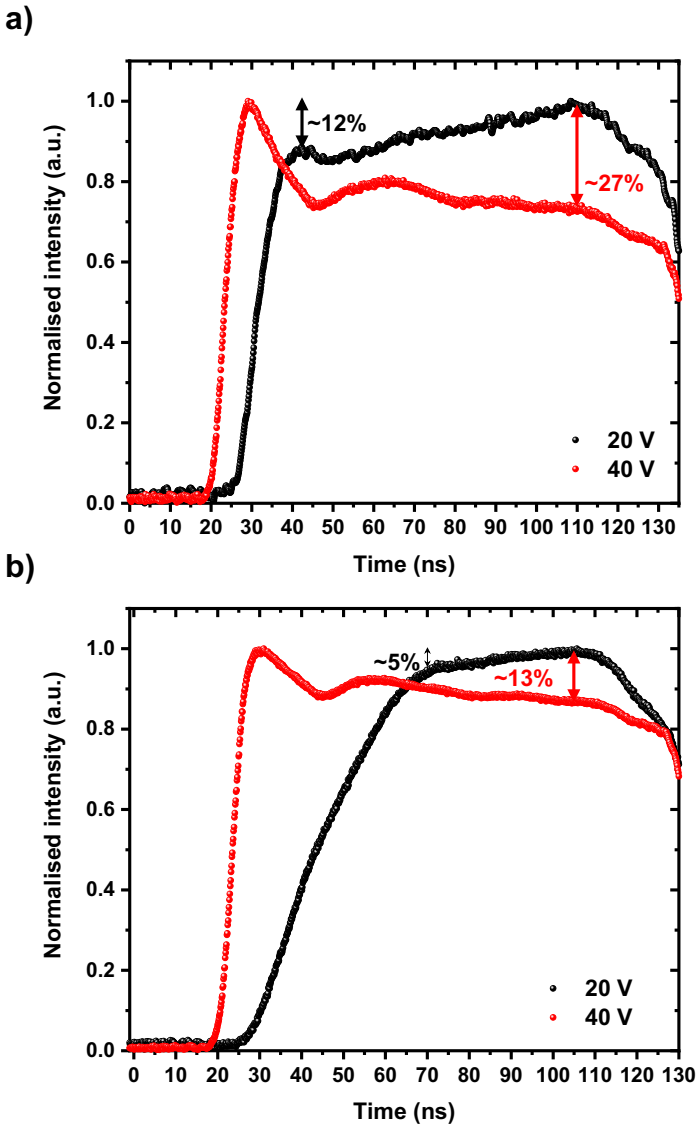

Figure 4. Transient electroluminescence (EL) response of (**a**) non-doped and (**b**) doped PCAN based OLEDs at bias of 20 V (black) and 40 V (red).

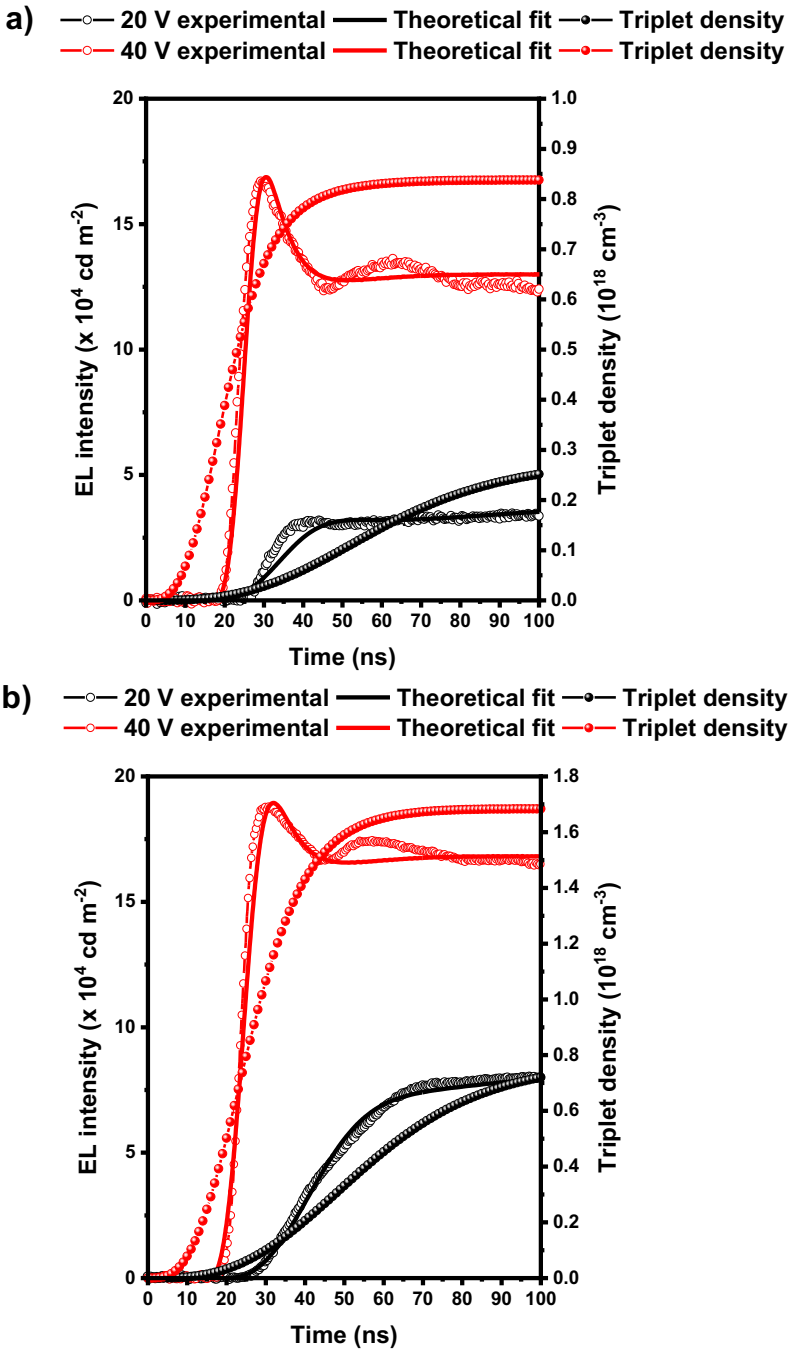

Figure 5. Experimental EL intensities overlapped with the theoretical fits and the corresponding triplet density extracted from the model for (**a**) non-doped and (**b**) doped PCAN based OLED at 20 (black) and 40 V (red).

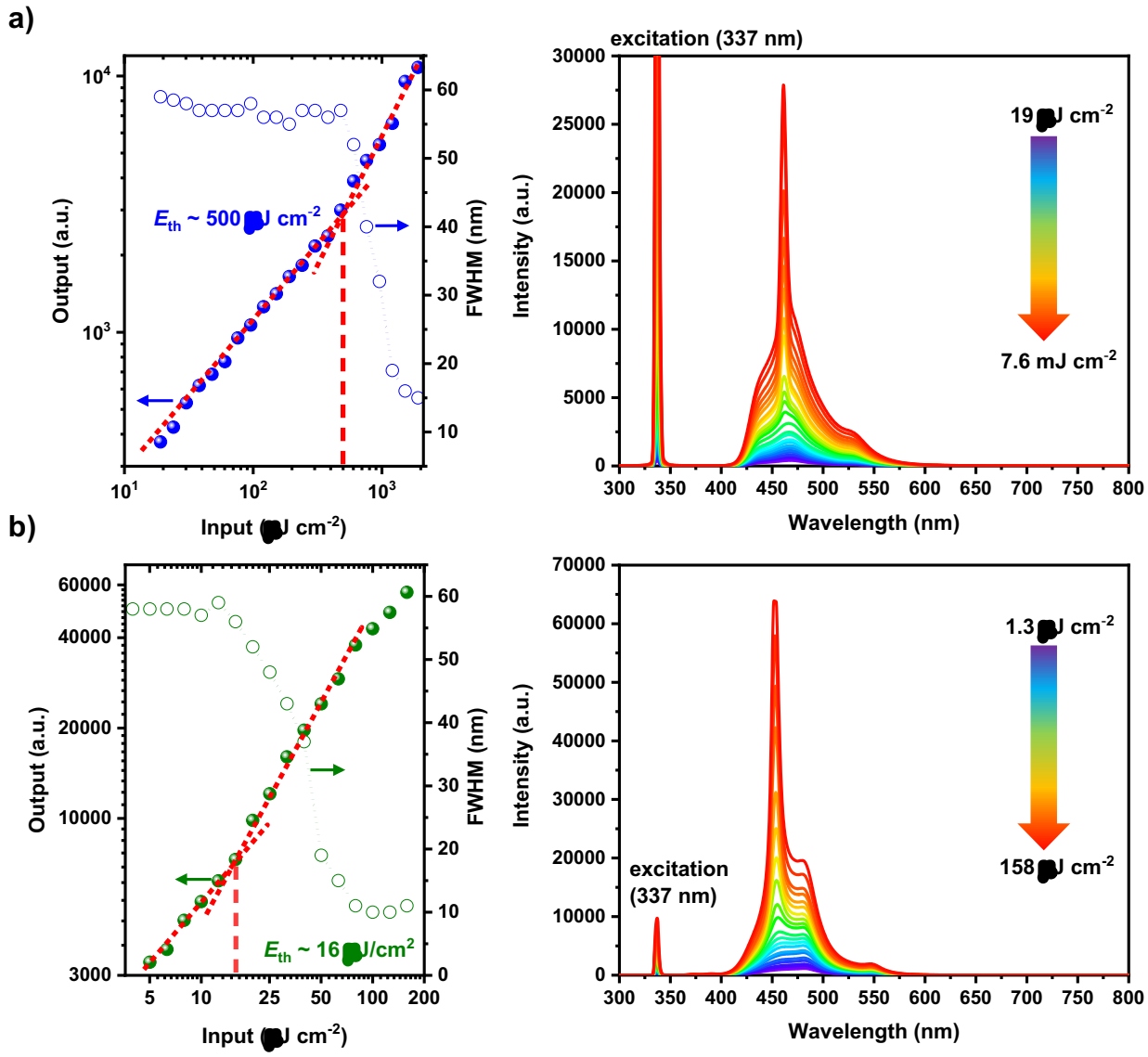

Figure 6. Input–output–FWHM and emission spectra collected from the edge of the organic layer at different input excitation intensities for (**a**) neat film and (**b**) doped films.

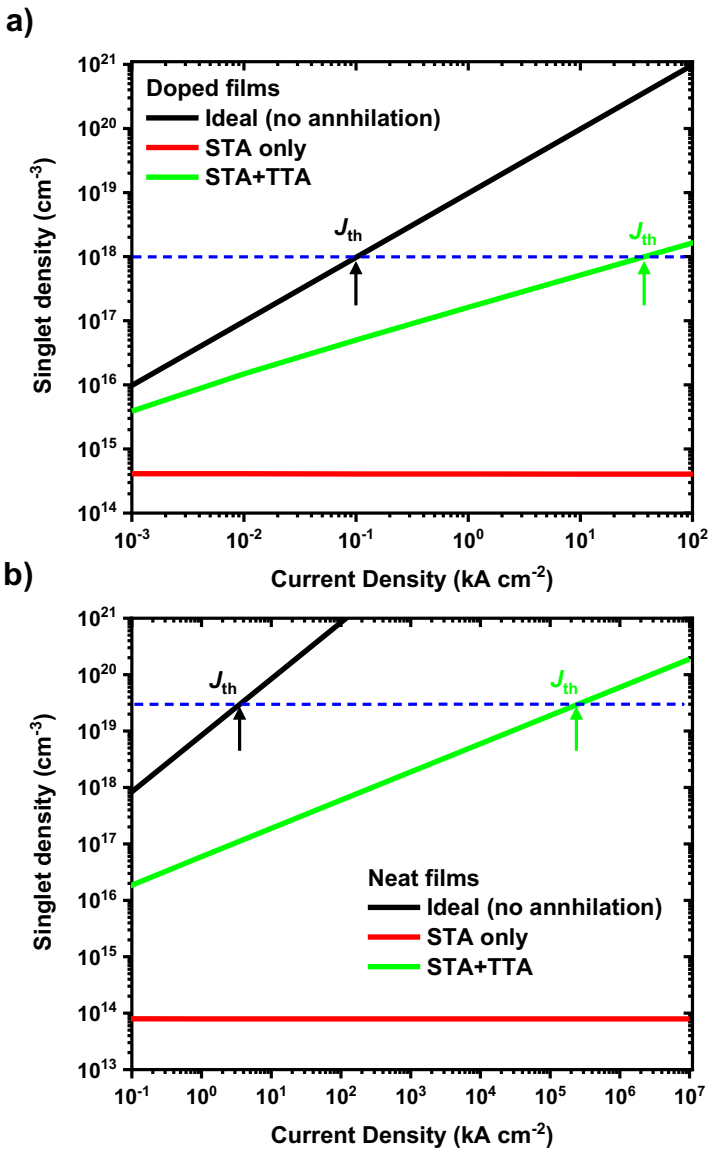

Figure 7. Simulated singlet exciton density as a function of current densities in all three conditions for (**a**) doped and (**b**) non-doped devices with blue line representing the singlet density at ASE threshold

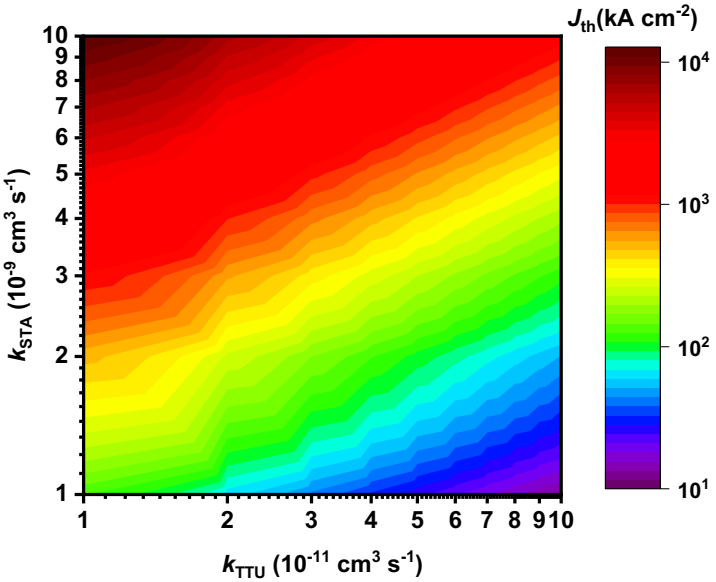

Figure 8. Variation of threshold current density as a function of STA and TTU rate constants

Figures

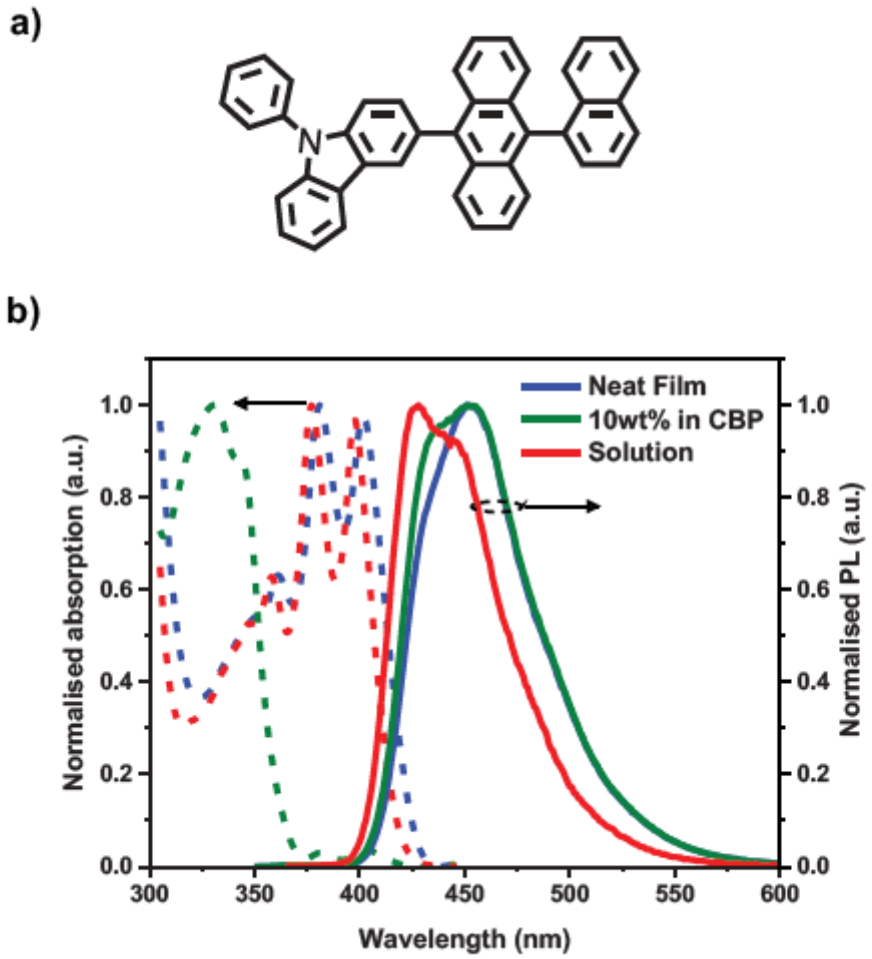

Figure 1

a) Chemical structure of PCAN. b) Normalised absorption (dashed lines) and PL (solid lines) spectra of PCAN in toluene solution (red), neat film (green) and 10wt% doped in CBP host matrix (blue).

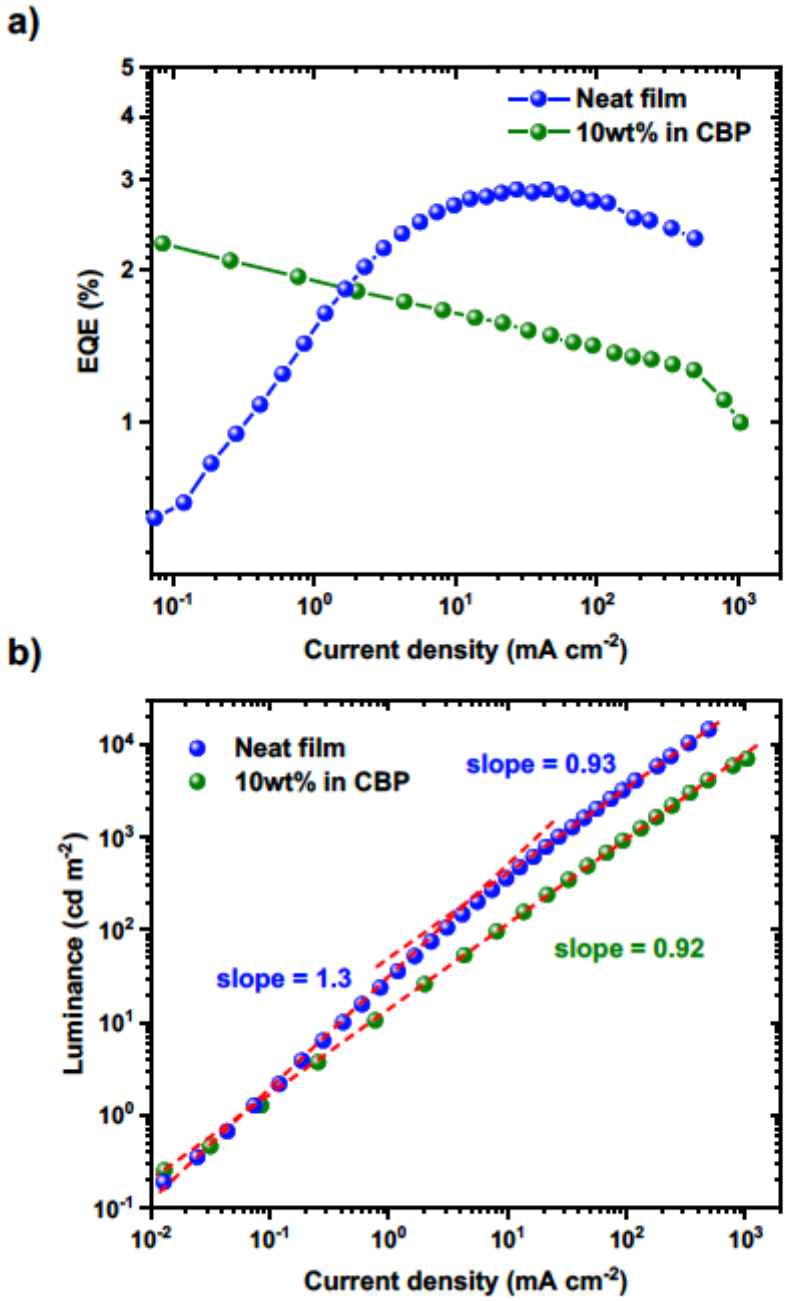

Figure 2

a) EQE vs current density and b) Luminance vs current density characteristics for OLEDs based on doped (green) and non-doped (blue) PCAN EMLs.

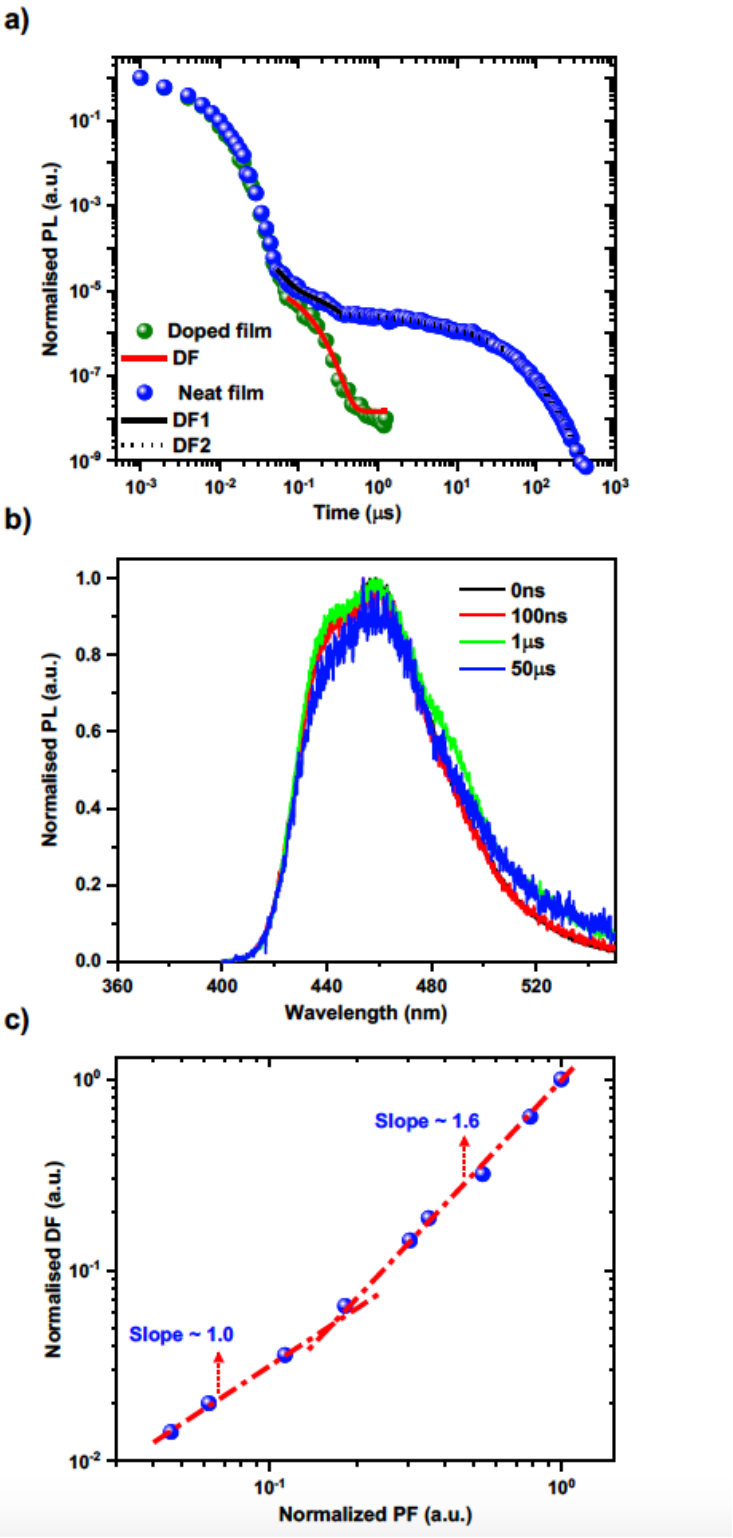

Figure 3

a) Time resolved emission decay for neat and doped films, b) emission spectra of neat films at different gate delays, c) Normalised DF intensities vs normalised PF intensities at different fluence for neat films, linearly fitted with dual slopes

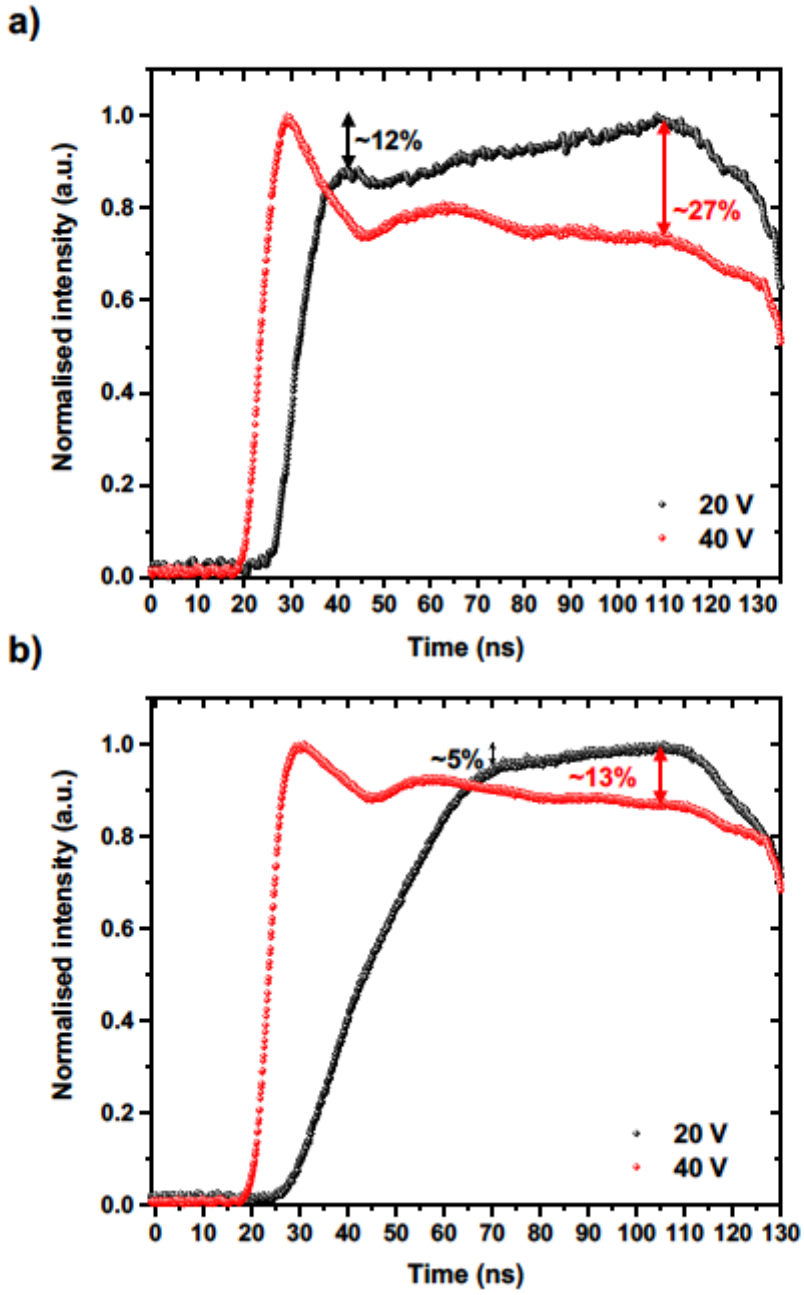

Figure 4

Transient electroluminescence (EL) response of (a) non-doped and (b) doped PCAN based OLEDs at bias of 20 V (black) and 40 V (red).

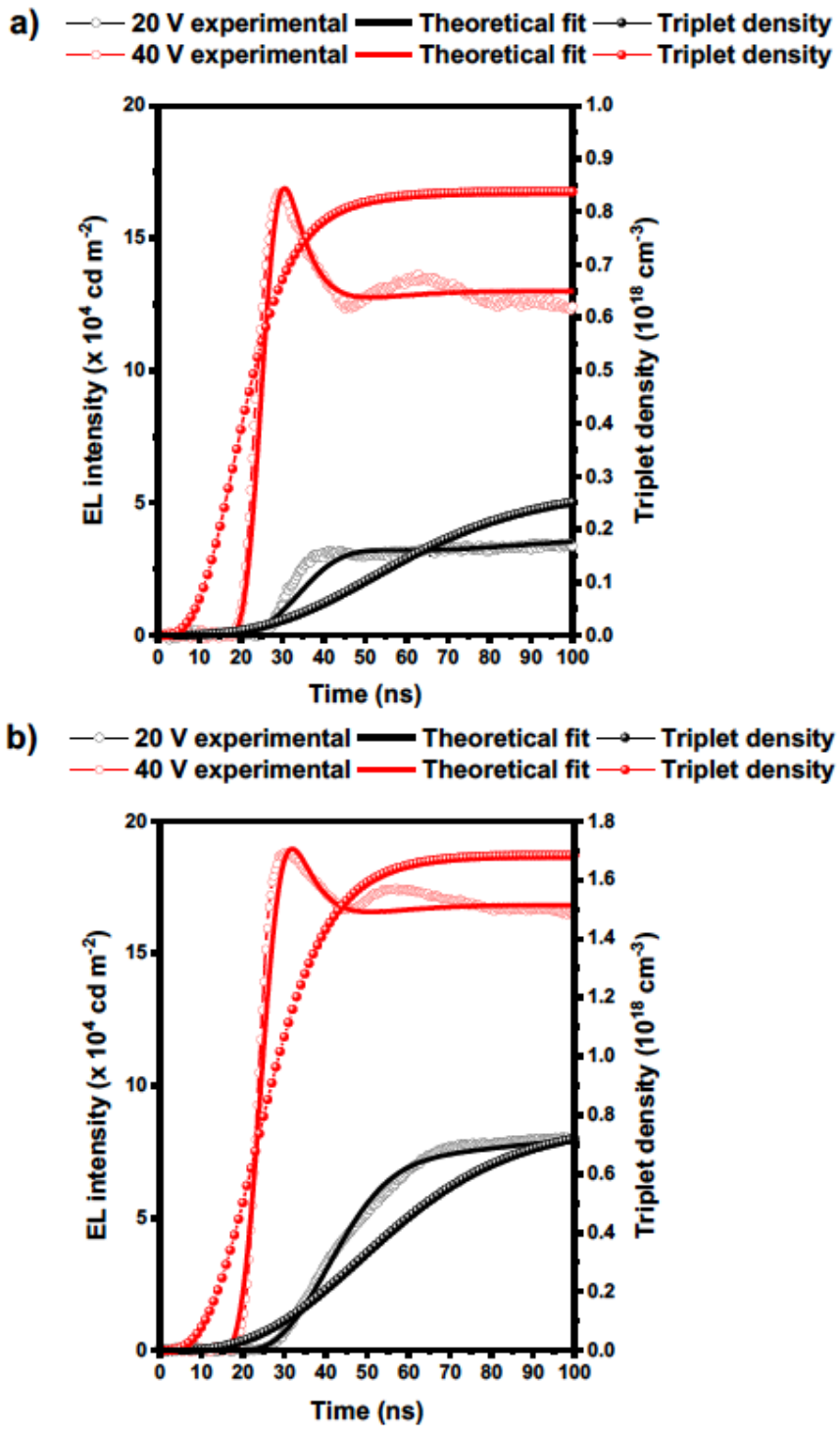

Figure 5

Experimental EL intensities overlapped with the theoretical fits and the corresponding triplet density extracted from the model for (a) non-doped and (b) doped PCAN based OLED at 20 (black) and 40 V (red).

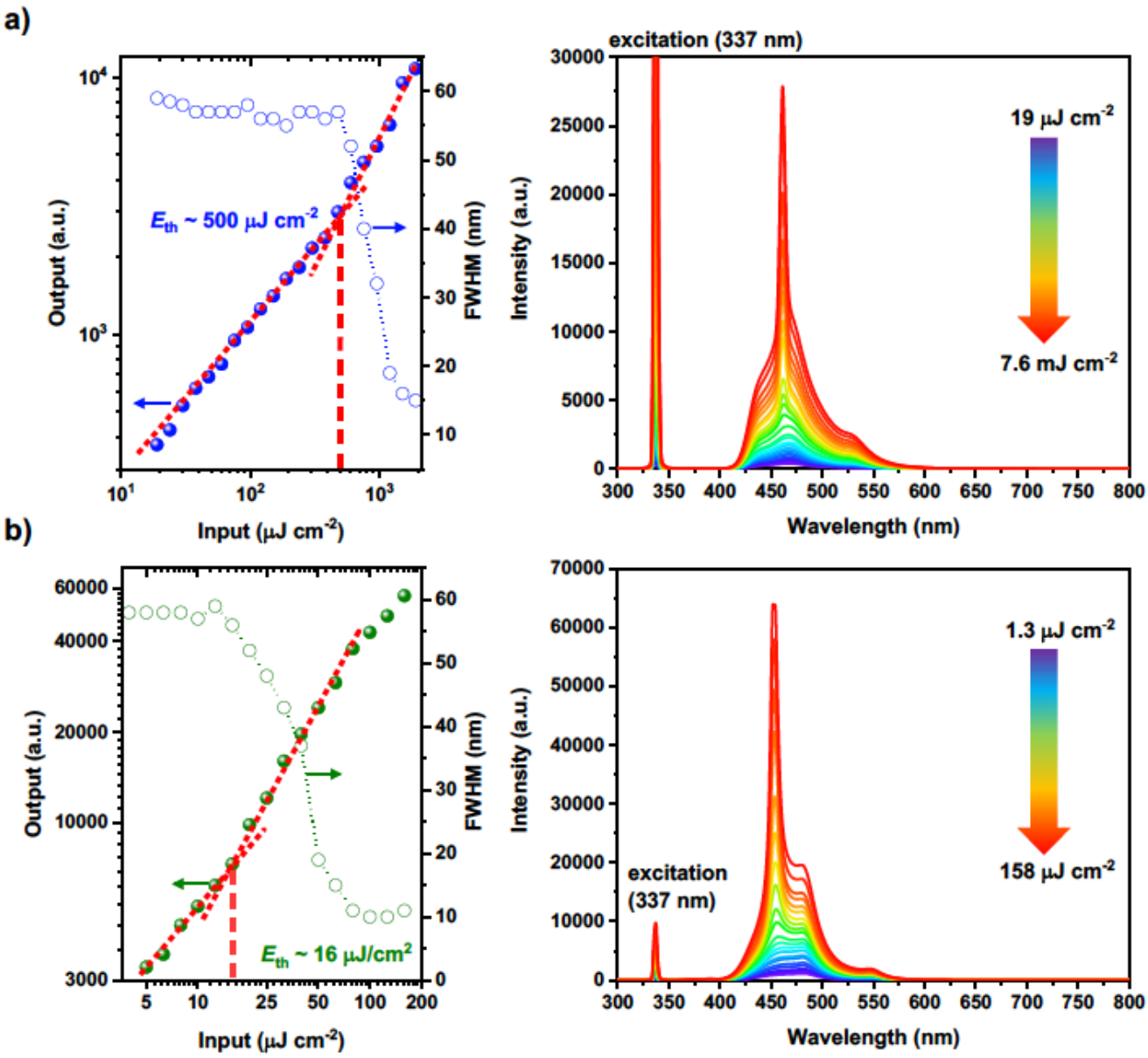

Figure 6

Input–output–FWHM and emission spectra collected from the edge of the organic layer at different input excitation intensities for (a) neat film and (b) doped films.

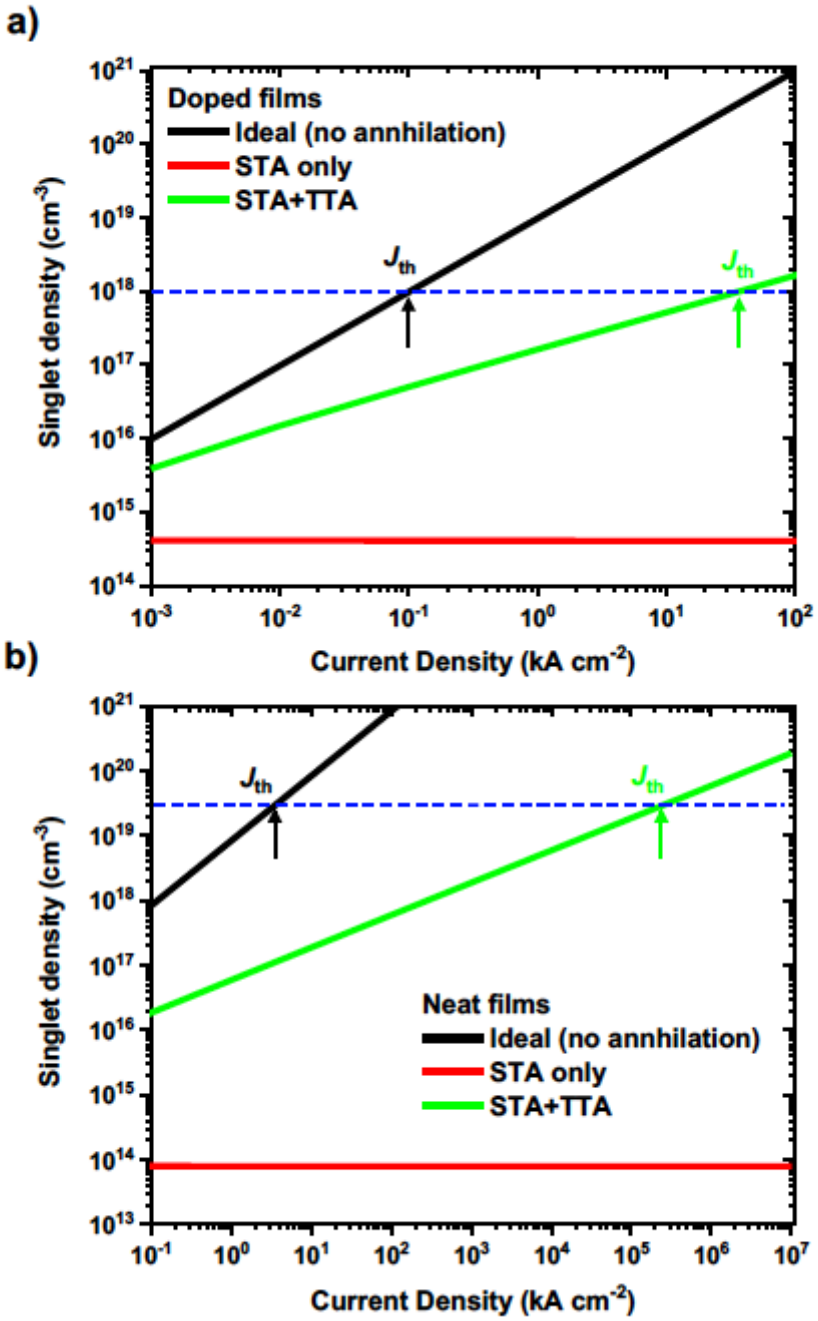

Figure 7

Simulated singlet exciton density as a function of current densities in all three conditions for (a) doped and (b) non-doped devices with blue line representing the singlet density at ASE threshold

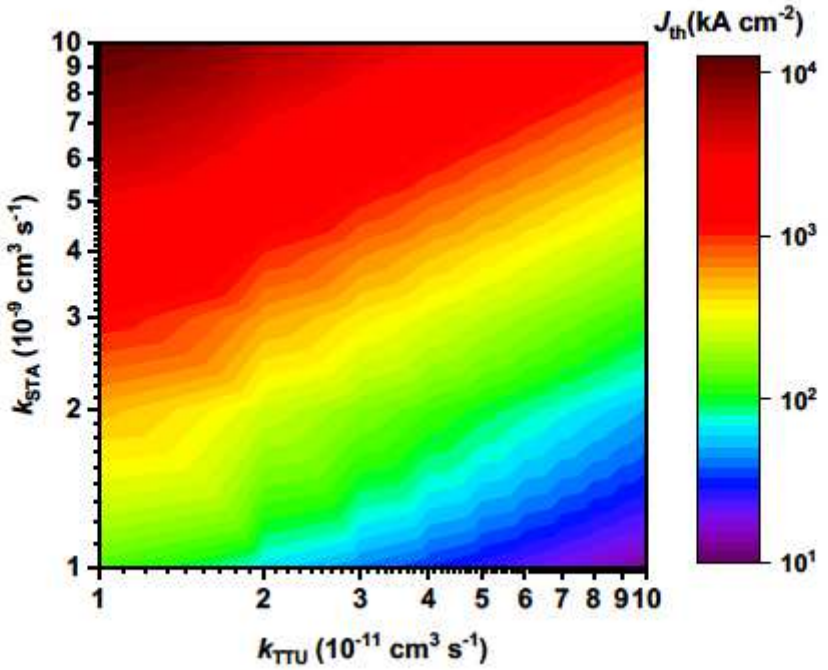

Figure 8

Variation of threshold current density as a function of STA and TTU rate constants

Supplementary Files

This is a list of supplementary files associated with this preprint. Click to download.

- SupportingInformationr.pdf